

Article

Synthesis, Crystal Structures and Catalytic Activities of Two Copper Coordination Compounds Bearing an *N,N'*-Dibenzylethylenediamine Ligand

Chao Liu *, Weiwei Zhang and Gaigai Cai

School of Chemistry and Chemical Engineering, Suzhou University, Suzhou 234000, China; hgzhangweiwei@stu.ahszu.edu.cn (W.W.Z.); hgcaigaigai@stu.ahszu.edu.cn (G.G.C.)

* Correspondence: kykrlu@ahszu.edu.cn; Tel.: +86-557-2875018

Received: 25 May 2020; Accepted: 17 June 2020; Published: 21 June 2020



Abstract: Two copper coordination compounds bearing an *N,N'*-dibenzylethylenediamine ligand, namely $[\text{Cu}_3\text{L}(\text{CH}_3\text{COO})_6]_n$ (**1**) and $[(\text{CuCl}_4)\cdot(\text{C}_6\text{H}_5\text{CH}_2\text{NH}_2\text{CH}_2)_2]$ (**2**) (L = *N,N'*-dibenzylethylenediamine) were synthesized by the ethanol refluxing method. Powder X-ray diffraction (PXRD), infrared spectra (IR), elemental analyses, and single crystal X-ray diffraction were used to characterize and verify their structures. Structural analyses showed that the asymmetric unit of compound (**1**), composed of two Cu(II) cations, three acetate anions, and half of the ligand, was bridged by one acetate to obtain an infinite 1D chain structure. The analyses further showed that the asymmetric unit of compound (**2**), composed of two crystallographically independent $[\text{C}_6\text{H}_5\text{CH}_2\text{NH}_2\text{CH}_2]^+$ units, four chloride anions, and one central Cu(II) cation is connected into an infinite 2D network structure by the hydrogen bonding interactions. The copper compounds were used to catalyze the decomposition of H_2O_2 , and the results showed that both of the compounds exhibited excellent catalytic activities under optimized conditions.

Keywords: *N,N'*-dibenzylethylenediamine; crystal structure; catalyst; coordination compound

1. Introduction

Among transition metal coordination compounds, copper coordination compounds occupy a vital position in organometallic chemistry due to their abundant coordination structures and potential applications in various fields [1–5]. In recent years, the catalytic activities of copper coordination compounds with various organic ligands have attracted extensive attention from chemists [6–9]. To develop novel and efficient catalysts, copper ions coordinated to a suitable ligand with multiple coordination sites and strong coordination abilities have been assembled into different copper coordination compounds [10,11]. Diamine and its derivatives are an important class of organic compounds with highly flexible *N,N*-donor atoms that can coordinate to different metal ions, thus producing a variety of mononuclear [12–14], binuclear [15–17], and polynuclear metal coordination compounds with excellent catalytic activities [18–20].

Hydrogen peroxide is a kind of oxidant [21], bleaching agent [22], and disinfectant [23] that is widely used in pharmaceutical, textile and chemical industries. [24–26]. As a result of the excessive use of H_2O_2 , local soil and water resources have become severely polluted [27]. Therefore, it is particularly important to develop a practical catalytic system for the decomposition of H_2O_2 . Presently, metal oxides, metal salts, and some coordination compounds have been used to catalyze the decomposition reaction of H_2O_2 , and considerable results have been obtained [28–30]. In order to better catalyze the decomposition of H_2O_2 , practical and efficient catalytic systems have become a research hotspot for chemical workers [31].

Therefore, the challenge we faced was to determine how to obtain coordination compounds with strong catalytic activities and low environmental pollution potential. With this purpose, we designed

and synthesized two novel copper coordination compounds bearing an *N,N'*-dibenzylethylenediamine ligand. Simultaneously, the catalytic activities of the coordination compounds were investigated for the decomposition reaction of H_2O_2 under mild conditions.

2. Materials and Methods

2.1. General Considerations

$(\text{NH}_4)_2\text{CuCl}_4 \cdot 2\text{H}_2\text{O}$ and *N,N'*-dibenzylethylenediamine were obtained from Shanghai Aladdin Bio-Chem Technology Co., Ltd. in Shanghai, China. Other reagents, such as KMnO_4 , H_2O_2 , $\text{Cu}(\text{OAc})_2 \cdot \text{H}_2\text{O}$, and $\text{CuCl}_2 \cdot 2\text{H}_2\text{O}$, were obtained from commercial sources and were used as received.

An FTS-40 spectrometer (Bio-Rad, Santa Clara, CA, USA) with a KBr pellet was used to collect the FT-IR spectra of the compounds in the $400\text{--}4000\text{ cm}^{-1}$ range. A DX-2600 diffractometer (Dandong, Liaoning, China) with $\text{Cu-K}\alpha$ radiation was employed to obtain powder X-ray diffractions at ambient temperature. A Vario Micro Cube elemental analyzer (Elementar, Frankfurt, Germany) was used to test the elemental analyses of compounds (1) and (2).

2.2. Synthesis of $[\text{Cu}_3\text{L}(\text{CH}_3\text{COO})_6]_n$ (1)

An ethanol (30 mL) solution of $\text{Cu}(\text{OAc})_2 \cdot \text{H}_2\text{O}$ (1.27 g, 2.12 mmol) was added to a 100 mL round-bottom flask with an ethanol (10 mL) solution of *N,N'*-dibenzylethylenediamine (0.50 mL, 2.12 mmol). The reaction solution was stirred and heated at $78\text{ }^\circ\text{C}$ for 24 h and the solution color gradually changed from light blue to deep blue. The reaction solvent was evaporated by vacuum distillation and the residue was carefully washed with *n*-hexane ($2 \times 5\text{ mL}$). The resulting solid was extracted with a co-solvent of dichloromethane and ethanol (8 mL, $V_{\text{dichloromethane}}/V_{\text{ethanol}} = 1/1$). The blue crystalline solid of compound (1) was obtained upon standing the resulting solution for 48 h at room temperature in a 64% yield. Melting point: $215.0\text{--}216.5\text{ }^\circ\text{C}$. Anal. Calcd. for $\text{C}_{28}\text{H}_{38}\text{Cu}_3\text{N}_2\text{O}_{12}$ (Formula weight = 785.22): C, 42.83; H, 4.88; N, 3.57%; Found: C, 42.64; H, 5.11; N, 3.79%. IR (KBr, cm^{-1}): 3426(s), 3066(w), 2978(m), 2924(s), 2765(s), 2689(m), 2568(m), 2404(m), 1564(s), 1400(s), 1301(w), 1023(m), 908(s), 842(w), 799(m), 744(s), 695(m), 646(s), 504 (w).

2.3. Synthesis of $[(\text{CuCl}_4) \cdot (\text{C}_6\text{H}_5\text{CH}_2\text{NH}_2\text{CH}_2)_2]$ (2)

An ethanol (30 mL) solution of $\text{CuCl}_2 \cdot 2\text{H}_2\text{O}$ (0.72 g, 4.24 mmol) was added to a 100 mL round-bottom flask with an ethanol (10 mL) solution of *N,N'*-dibenzylethylenediamine (1.00 mL, 4.24 mmol). After being added to two drops of diluted hydrochloric acid under stirring, the reaction solution was stirred and heated at $78\text{ }^\circ\text{C}$ for 24 h; as a result, the solution color gradually changed from light blue to deep blue. The reaction solvent was evaporated by vacuum distillation and the residue was carefully washed with *n*-hexane ($2 \times 5\text{ mL}$). The resulting solid was extracted with a co-solvent of *n*-hexane and methanol (12 mL, $V_{\text{n-hexane}}/V_{\text{methanol}} = 1/2$). The blue crystalline solid of compound (2) was obtained upon standing the resulting solution for 24 h at room temperature in a 79% yield. Melting point: $189.5\text{--}190.5\text{ }^\circ\text{C}$. Anal. Calcd. for $\text{C}_{16}\text{H}_{22}\text{Cl}_4\text{CuN}_2$ (Formula weight = 447.69): C, 42.92; H, 4.95; N, 6.26%; Found: C, 43.21; H, 5.03; N, 6.06%. IR (KBr, cm^{-1}): 3443(s), 3055(w), 2902(m), 2847(w), 2771(m), 2361(s), 2334(m), 1640(s), 1591(s), 1553(s), 1487(m), 1411(s), 1148(m), 1066 (m), 1023(m), 974(w), 842(w), 739(m), 701(s), 684(m), 631(w).

2.4. X-ray Crystallography

Single crystals with dimensions of $0.10 \times 0.12 \times 0.14\text{ mm}$ for compound (1) and $0.22 \times 0.25 \times 0.27\text{ mm}$ for compound (2) were selected for single-crystal X-ray diffraction analyses on a Bruker APEX-II CCD diffractometer (Bruker, Karlsruhe, Germany). The diffraction data were collected by graphite monochromated Mo-K α radiation ($\lambda = 0.71073\text{ \AA}$) at $296(2)\text{ K}$. The empirical absorption corrections were performed using the SADABS program. The crystal structures of compounds (1) and (2) were solved by direct methods using the SHELXT program [32] and were refined by full-matrix least-squares on F^2 with

the SHELXL 2018/3 program [33]. All non-hydrogen atoms were refined anisotropically and the hydrogen atoms were placed in the geometrically idealized positions. The crystallographic data for the compounds are given in Table 1. The selected bond lengths (Å) and angles (°) of the compounds are summarized in Table S1 in Supplementary Materials.

Table 1. Crystallographic data for compounds (1) and (2).

Compound	(1)	(2)
Formula	C ₂₈ H ₃₈ Cu ₃ N ₂ O ₁₂	C ₁₆ H ₂₂ C ₁₄ CuN ₂
Formula weight	785.22	447.69
Temperature	296(2)	296(2)
Crystal system	Monoclinic	Triclinic
Space group	C2/c	P $\bar{1}$
<i>a</i> (Å)	15.903(13)	6.5935(9)
<i>b</i> (Å)	16.403(15)	11.9953(18)
<i>c</i> (Å)	15.679(12)	12.4736(17)
α	90.00	84.199(4)
β	96.06(2)	88.408(4)
γ	90.00	77.972(4)
Volume (Å ³)	4067(6)	959.9(2)
Z	4	2
Density (calculated)/(g·cm ⁻³)	1.283	1.549
μ (mm ⁻¹)	1.605	1.694
<i>F</i> (000)	1612	458
Reflections collected	13,134	6888
Unique reflections (<i>R</i> _{int})	4648 (0.064)	3346 (0.040)
Gof	1.026	1.057
Final <i>R</i> indices [<i>I</i> > 2 σ (<i>I</i>)]	<i>R</i> ₁ = 0.0931, <i>wR</i> ₂ = 0.2708	<i>R</i> ₁ = 0.0300, <i>wR</i> ₂ = 0.0770
<i>R</i> indices (all data)	<i>R</i> ₁ = 0.1098, <i>wR</i> ₂ = 0.2899	<i>R</i> ₁ = 0.0322, <i>wR</i> ₂ = 0.0786
Largest diff. peak and hole (e Å ⁻³)	0.96 and -1.13	0.30 and -0.49

2.5. Decomposition Reaction of Hydrogen Peroxide

A synthesized compound (1.0 mmol) was added to a 50 mL round-bottom flask with *N,N*-dimethylformamide (DMF) (5 mL). An aqueous solution of H₂O₂ (10 mL, 30 wt %) was diluted 2 times with distilled water (10 mL) and carefully injected into the round-bottom flask. The decomposition reaction proceeded at room temperature for 24 h and the solution gradually became slightly turbid. The reaction process was monitored by hydrogen peroxide test paper. In order to measure the decomposition percentage of H₂O₂ in the presence of the catalyst, the residual H₂O₂ concentration was titrated by using a standard solution of KMnO₄ [34].

3. Results and Discussion

3.1. Structure Description of [Cu₃L(CH₃COO)₆]_n

The asymmetric unit of [Cu₃L(CH₃COO)₆]_n contains two Cu(II) cations, three acetate anions, and half of the ligand (Figure 1). The central Cu1 cation has the same coordination geometry as the Cu1 (ii) cation, where Cu1 cation is five-coordinated by five oxygen atoms (O2, O3, O5, O1(ii) and O6(ii)) from five different bridging acetates in an η^1 mode. This leads to a square pyramidal CuO₅ coordination geometry. The observed geometric parameter τ (0.003) reveals that the Cu1 cation lies in an almost perfect square pyramidal environment. The basal plane of the square pyramidal geometry is defined by four oxygen atoms (O2, O5, O1(ii), and O6(ii)) with Cu1–O bond lengths ranging from 1.976(5) to 1.989(5) Å, while the apical position is occupied by one oxygen atom (O3) from another acetate anion with the Cu1–O3 bond of 2.178(5) Å. The Cu1–O bond lengths of the basal plane were found to be shorter than the apical Cu1–O3 bond length, which indicates that they are more stable than the Cu1–O3 bond. When the bond angles O2–Cu1–O5 of 88.1(2)°, O2–Cu1–O6(ii) of

90.6(2)°, O1(ii)–Cu1–O6(ii) of 89.4(2)°, and O1(ii)–Cu1–O5 of 89.8(2)° were added, the sum equaled 357.9°, nearly equal to 360°, further confirming that the Cu1 cation is in an almost perfect square pyramidal environment. The adjacent Cu(II) cations (Cu1 and Cu1(ii)) are bridged by four acetates in a μ_2 - η^1 : η^1 -bridging coordination mode, forming a paddlewheel dinuclear $\text{Cu}_2(\text{CO}_2)_4$ building unit. The nonbonding Cu1 ... Cu1(ii) distance is 2.6274(16) Å, which is in agreement with those of some similar copper compounds [35,36]. The Cu2 cation is four-coordinated by two nitrogen atoms (N1 and N1(i)) from the N,N' -dibenzylethylenediamine ligand in an η^2 mode and two oxygen atoms (O4 and O4(i)) from two bridging acetates in η^1 mode. This results in a square-planar CuN_2O_2 coordination geometry. The average bond length of Cu2–O is 1.976(5) and that of Cu2–N is 2.007(5) Å, both of which correspond with the reported values [37,38]. The sums of the bond angles N1–Cu2–N1(i) of 85.1(2)°, O4(i)–Cu2–N1(i) of 94.7(2)°, O4–Cu2–O4(i) of 93.5(2)°, and O4–Cu2–N1 of 94.7(2)° when added up equal 368°, which is unequal to 360°, which confirms that the four-coordinated atoms and Cu2 cation are in an imperfect plane.

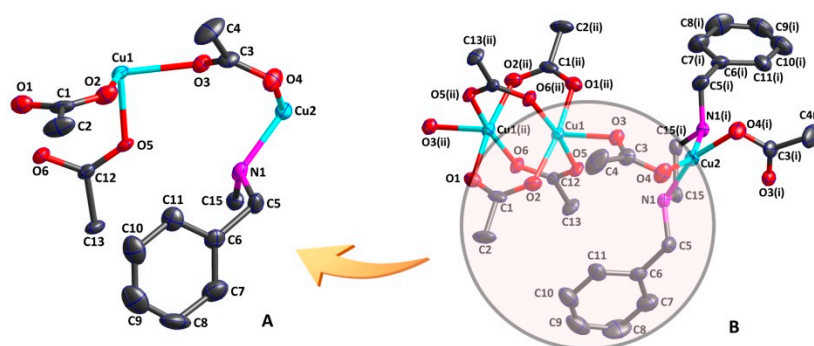


Figure 1. An asymmetric unit of compound (1) (A) and a secondary structure with a paddlewheel $\text{Cu}_2(\text{CO}_2)_4$ unit (B) (thermal ellipsoids at 30% probability level). Symmetry codes: (i) $1-x, y, 3/2-z$; (ii) $1/2-x, 3/2-y, 1-z$.

As shown in Figure 2, the CuN_2O_2 unit and the $\text{Cu}_2(\text{CO}_2)_4$ unit are bridged by one acetate in a μ_2 - η^1 : η^1 -bridging coordination mode, forming an infinite 1D chain along the a axis. In addition, there are weak intramolecular hydrogen bonds between the ligand and the acetate (Table S2). The nitrogen atom (N1) from the ligand acts as an H-donor to the oxygen atom (O5) from one acetate, forming the intramolecular hydrogen bond N1–H1 ... O5, which further stabilizes the 1D chain structure.

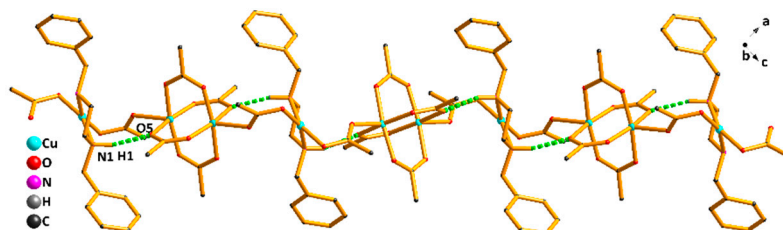


Figure 2. The 1D chain structure of compound (1).

3.2. Structure Description of $[(\text{CuCl}_4) \cdot (\text{C}_6\text{H}_5\text{CH}_2\text{NH}_2\text{CH}_2)_2]$

Figure 3 shows that the asymmetric unit of $[(\text{CuCl}_4) \cdot (\text{C}_6\text{H}_5\text{CH}_2\text{NH}_2\text{CH}_2)_2]$ consists of four chloride anions, one central Cu(II) cation, and two crystallographically independent $[\text{C}_6\text{H}_5\text{CH}_2\text{NH}_2\text{CH}_2]^+$ units. The Cu1 cation is four-coordinated by four chloride anions (Cl1, Cl2, Cl3, and Cl4) in η^1 mode, resulting in a distorted tetrahedral $[\text{CuCl}_4]^{2-}$ coordination geometry. The four Cu1–Cl bond lengths are 2.2529(7), 2.2199(7), 2.2648(7), and 2.2643(7) Å, respectively, none of which are equal to one another. The bond angles Cl3–Cu1–Cl4 of 91.80(2)°, Cl1–Cu1–Cl4 of 98.22(2)°, Cl1–Cu1–Cl2 of 96.54(2)°, and Cl2–Cu1–Cl3 of 102.21(2)° differ significantly from the standard tetrahedral angle of 109.5°. Both of the bond angles

(Cl2–Cu1–Cl4, which is $141.65(2)^\circ$, and Cl2–Cu1–Cl4, which is $135.02(2)^\circ$) are significantly greater than other Cl–Cu1–Cl bond angles. This indicates that the Cu1(II) cation is in a distorted tetrahedral coordination environment. However, the ligand does not coordinate to the Cu(II) cation; instead, it reacts with diluted hydrochloric acid to give its acid salt $[H_2L]^{2+}$. The acid salt $[H_2L]^{2+}$ assumes the role of the counter cation, which can balance the valence charge of the $[CuCl_4]^{2-}$ anion. Through the electrostatic interaction between positive and negative ions, the asymmetric unit is further stabilized.

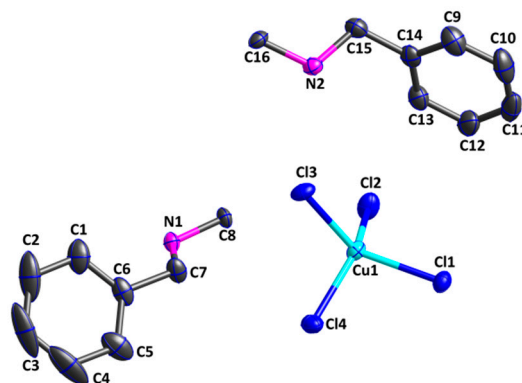


Figure 3. An asymmetric unit of compound (2) (thermal ellipsoids at 30% probability level).

Moreover, there is an abundance of intermolecular and intramolecular hydrogen bonds in compound (2) (Table S2) that benefit the stability of the crystal structure. As shown in Figure 4, the nitrogen atoms from the *N,N'*-dibenzylethylenediamine ligand act as an H-donor to the chlorine atoms from $[CuCl_4]^{2-}$ unit, forming the hydrogen bonds N1–H1A ... Cl1(iii) of 2.37 Å, N1–H1B ... Cl4(iv) of 2.51 Å, and N2–H2B ... Cl3(v) of 2.37 Å. The intermolecular hydrogen bonds play an important role in constructing the stable 1D chain structure of compound (2). Another noticeable characteristic of compound (2) is how the intermolecular hydrogen bonding interactions exist among 1D chains, such as N2–H2A ... Cl1(iv) of 2.81 Å and C16–H16B ... Cl4(v) of 2.82 Å. Under the weak hydrogen bonding interactions, the 1D chain structure is further connected and extended, resulting in an infinite 2D network structure in Figure 5.

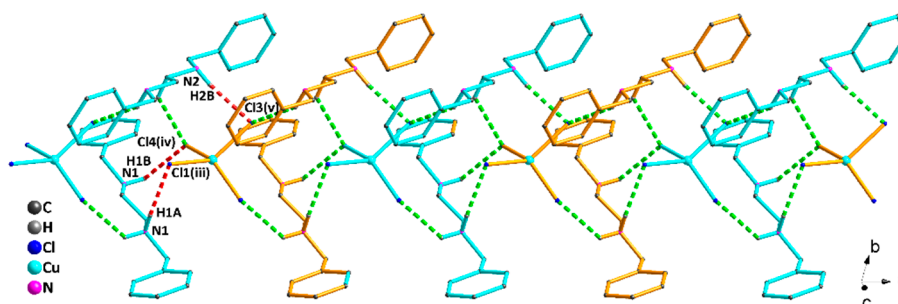


Figure 4. The 1D chain structure of compound (2). Symmetry codes: (iii) $1-x, -y, 1-z$; (iv) $1+x, y, z$; (v) $1-x, 1-y, 1-z$.

3.3. PXRD Analysis

To verify the phase purities of the crystal samples, PXRD experiments were further carried out on compounds (1) and (2) at room temperature. The simulated and experimental PXRD patterns for compounds (1) and (2) are presented in Figures S1 and S2, respectively. The peaks in the experimental curves matched with those in the simulated curves generated from the single crystal X-ray data, thus confirming that the phase purities of the synthesized compounds are correct. The reflection intensities of the experimental patterns were not in agreement with the corresponding simulated patterns; this may be attributed to the different orientations of the crystal samples during the

test. Additionally, the elemental analyses of compounds (1) and (2) support the results of the PXRD experiments.

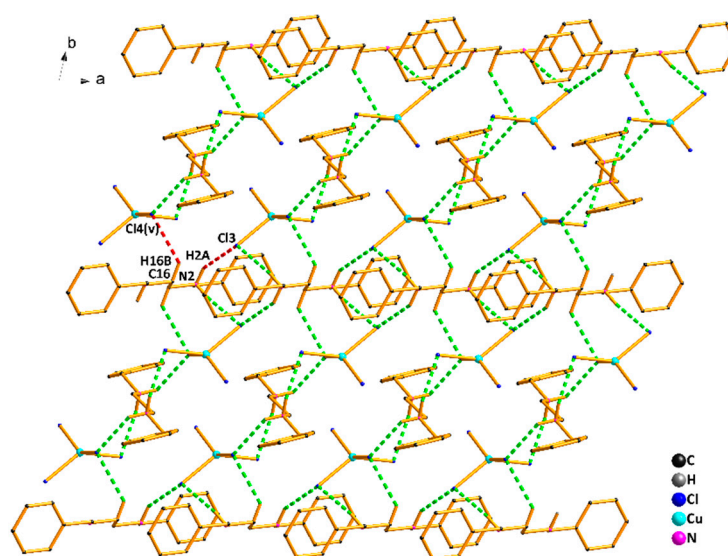


Figure 5. The 2D network structure of compound (2). Symmetry codes: (iii) $1-x, -y, 1-z$; (iv) $1+x, y, z$; (v) $1-x, 1-y, 1-z$.

3.4. Catalytic Activities of the Compounds

Hydrogen peroxide, which has severely polluted local soil and water sources because of its extensive use in production and life, could instead be efficiently decomposed under the catalysis of metal compounds [28–30]. To optimize the favorable reaction conditions, such as the pH value and catalyst loading, the decomposition reaction of H_2O_2 catalyzed by the synthesized compounds was carried out under different conditions. The results are given in Tables 2 and 3.

Firstly, the decomposition reaction of H_2O_2 with compound (1) as a catalyst with the pH value of 8 was used as a model reaction to evaluate the effect of the catalyst loading on this reaction. When the catalyst loading was 1.0 mmol, the decomposition rate of H_2O_2 reached 94% (Entry 3). Although the decomposition reaction may efficiently occur under the catalysis of compound (1) with a catalyst loading range between 1.0 and 1.6 mmol, the decomposition rate remained almost unchanged (Entries 3–5), which implied that an excessive amount of catalyst could not effectively improve the decomposition rate. When the catalyst loading was reduced from 1.0 to 0.4 mmol, the decomposition percentage decreased significantly from 94 to 39% (Entries 1–3). The experimental data revealed that H_2O_2 could not be fully decomposed with the catalyst loading below 1.0 mmol. In comparison with compound (1), compound (2) exhibited stronger catalytic activities in catalyzing the decomposition of H_2O_2 . Surprisingly, when the loading of compound (2) was 1.0 mmol, the decomposition percentage reached nearly 100% (i.e., 99%) (Entry 8). In addition, regardless of the loading of compound (2) was increased or decreased, the decomposition percentage of H_2O_2 had the same rule as compound (1) (Entries 6 and 7, 9 and 10). Therefore, the most suitable catalyst loading was 1.0 mmol, and thus was selected for the following studies. The catalytic activities of the N,N' -dibenzylethylenediamine ligand were also explored. As we expected, the residual concentration of H_2O_2 remained almost constant (Entry 11), which confirmed that the ligand had no catalytic activities in the decomposition reaction. According to the related literature [39], $\text{CuCl}_2 \cdot 2\text{H}_2\text{O}$ and $\text{Cu}(\text{OAc})_2 \cdot \text{H}_2\text{O}$ are also excellent catalysts in the decomposition of H_2O_2 . We found that the decomposition percentages of 84% and 77% were obtained with a catalyst loading of 1.0 mmol, respectively (Entries 12 and 13). The copper metal contents of $\text{CuCl}_2 \cdot 2\text{H}_2\text{O}$ and $\text{Cu}(\text{OAc})_2 \cdot \text{H}_2\text{O}$ were higher than those of the synthesized compounds, and thus may cause more serious environmental damage. The catalytic activities of $(\text{NH}_4)_2\text{CuCl}_4 \cdot 2\text{H}_2\text{O}$ were also surveyed (Entry 14), and from this, we found that the decomposition percentage of 81%,

which is lower than the 99% of compound (2), proved that the ligand unit in this compound also plays an important role in the catalytic process.

Table 2. The effects of catalyst loading on the decomposition reaction of H₂O₂.

Entry	Catalyst	Catalyst Loading (mmol)	Decomposition Percent (%)
1	compound (1)	0.4	39
2		0.7	78
3		1.0	94
4		1.3	95
5		1.6	95
6	compound (2)	0.4	44
7		0.7	82
8		1.0	99
9		1.3	99
10		1.6	99
11	Ligand	1.0	0
12	Cu(OAc) ₂ ·H ₂ O	1.0	77
13	CuCl ₂ ·2H ₂ O	1.0	84
14	(NH ₄) ₂ CuCl ₄ ·2H ₂ O	1.0	81

To study the effect of pH levels on the rate of the decomposition of H₂O₂, we tested the catalytic activities of the coordination compounds with a catalyst loading of 1.0 mmol under different pH conditions. We found that the pH value of the solution had a considerable influence on the catalytic activities of the coordination compounds. Under acidic conditions, the catalytic activities of the coordination compounds were very poor (Entries 1 and 2, 5 and 6), but the catalytic activities strengthened significantly with the increase in pH value. When the solution was weakly alkaline, such as at pH 8, the decomposition percentages of H₂O₂ reached 94% and 99%, respectively (Entries 4 and 10). The experimental results showed that when the pH value of the solution was higher than 9, the decomposition rate of H₂O₂ decreased significantly; this may be due to the side reactions between the compounds and the hydroxyl ion. We concluded that the weak alkaline solution with the pH value of 8 is suitable for the decomposition of H₂O₂.

Table 3. The effect of pH on the decomposition reaction of H₂O₂.

Entry	Catalyst	pH	Decomposition Percent (%)
1	compound (1)	5	44
2		6	65
3		7	81
4		8	94
5		9	88
6		10	79
7	compound (2)	5	51
8		6	69
9		7	86
10		8	99
11		9	80
12		10	61

Considering the decomposition rate and the concepts of green chemistry, compound (2) rather than compound (1) and the copper salts was found to be a more suitable catalyst with a catalyst loading of 1.0 mmol and a pH value of 8 for the decomposition reaction of H₂O₂.

4. Conclusions

In this study, two copper coordination compounds bearing an *N,N'*-dibenzylethylenediamine ligand were synthesized. The crystal structure of compound (1) revealed that the Cu1 cation, as well as the Cu1(ii) cation, lies in an almost perfect square pyramidal CuO₅ coordination environment and that the Cu2 cation lies in a distorted square planar CuN₂O₂ coordination geometry. Both the CuN₂O₂ unit and the Cu₂(CO₂)₄ unit were bridged to generate an infinite 1D chain structure by the bidentate acetate. The crystal structure of compound (2) revealed that the Cu1(II) cation forms a distorted tetrahedral [CuCl₄]²⁻ coordination environment. Two [C₆H₅CH₂NH₂CH₂]⁺ units and the [CuCl₄]²⁻ anion constituted the asymmetric unit of compound (2), which is further connected to an infinite 2D network structure via the hydrogen bonding interactions. In addition, examination on their catalytic activities indicated that compounds (1) and (2) with a catalyst loading of 1.0 mmol and a pH value of 8 could efficiently catalyze the decomposition of H₂O₂. Considering the decomposition rate and the concepts of green chemistry, compound (2) is a more suitable catalyst for the decomposition of H₂O₂ than compound (1).

Supplementary Materials: The following are available online at <http://www.mdpi.com/2073-4352/10/6/528/s1>: Selected bond lengths (Å) and angles (°) of compounds (1) and (2); Table S2. Hydrogen bonding parameters for compounds (1) and (2); Figure S1. PXRD patterns of compound (1); Figure S2. PXRD patterns of compound (2). CCDC-1988490 for compound (1) and CCDC-1988519 for compound (2).

Author Contributions: Conceptualization, C.L.; methodology, C.L.; investigation, W.Z.; funding acquisition, C.L.; project administration, G.C.; formal analysis, W.Z.; writing—original draft preparation, C.L.; writing—review and editing, C.L. and G.C. All authors have read and agreed to the published version of the manuscript.

Funding: This work was funded by the National Natural Science Foundation of China (No. 21977001), the Academic Leader Program of Suzhou University (No. 2018XJHB02), and the Innovation and Entrepreneurship Training Program for College Students in Anhui Province (No. 201910379079).

Acknowledgments: The authors would like to thank Anhui Medical University and Anhui Key Laboratory of Spin Electron and Nanomaterials for the characterization of the compounds.

Conflicts of Interest: The authors declare no conflicts of interest.

References

1. Wang, H.; Sorolla, M.; Wang, X.; Jacobson, A.J.; Wang, H.; Pillai, A.K. Synthesis, crystal structures and in vitro anticancer activities of two copper(II) coordination compounds. *Transit. Met. Chem.* **2018**, *44*, 237–245. [[CrossRef](#)]
2. Călinescu, M.; Fiastru, M.; Bala, D.; Mihailciuc, C.; Negreanu-Pîrjol, T.; Jurcă, B. Synthesis, characterization, electrochemical behavior and antioxidant activity of new copper(II) coordination compounds with curcumin derivatives. *J. Saudi Chem. Soc.* **2019**, *23*, 817–827. [[CrossRef](#)]
3. Sran, B.S.; Sharma, S.; Hundal, G. Self-assembly and supramolecular isomerism in copper (II) coordination compounds of pyridine-4-carboxamide based ligand. *Inorg. Chim. Acta* **2018**, *486*, 74–82. [[CrossRef](#)]
4. He, G.; Li, J.; Wang, Z.; Liu, C. Synthesis of a fluorogenic probe for thiols based on a coumarin schiff base copper complex and its use for the detection of glutathione. *Tetrahedron* **2017**, *73*, 272–277. [[CrossRef](#)]
5. Wang, Y.; Li, S.; Wang, L.; Qu, S.; Liu, K. Geometric relaxation in a copper complex and its limitation by polymer immobilization: Structure, characterization and photophysical analysis. *J. Lumin.* **2017**, *192*, 269–276. [[CrossRef](#)]
6. Muthukumar, P.; Pannipara, M.; Al-Sehemi, A.G.; Moon, D.; Anthony, S.P. Polymorphs of a copper coordination compound: Interlinking active sites enhance the electrocatalytic activity of the coordination polymer compared to the coordination complex. *CrystEngComm* **2020**, *22*, 425–429. [[CrossRef](#)]
7. Zhao, N.; Li, Y.; Gu, J.; Fernandes, T.A.; Kirillova, M.V.; Kirillov, A.M. New copper(II) coordination compounds assembled from multifunctional pyridine-carboxylate blocks: Synthesis, structures, and catalytic activity in cycloalkane oxidation. *Molecules* **2018**, *24*, 6. [[CrossRef](#)]
8. Amini, M.; Nikkhoo, M.; Tekantappeh, S.B.; Farniab, S.M.F.; Mahmoudi, G.; Büyükgüngör, O. Synthesis, characterization and catalytic properties of a copper complex containing decavanadate nanocluster, Na₂[Cu(H₂O)₆]₂[V₁₀O₂₈·4H₂O]. *Inorg. Chem. Commun.* **2017**, *77*, 72–76. [[CrossRef](#)]

9. Sindhuja, D.; Vasanthakumar, P.; Bhuvanesh, N.; Karvembu, R. Catalytic assessment of copper(I) complexes and a polymer analog towards the one-pot synthesis of imines and quinoxalines. *Eur. J. Inorg. Chem.* **2019**, *2019*, 3940–3941. [[CrossRef](#)]
10. Nesterova, O.V.; Bondarenko, O.E.; Pombeiro, A.J.L.; Nesterov, D.S. Phenoxazinone synthase-like catalytic activity of novel mono- and tetranuclear copper(II) complexes with 2-benzylaminoethanol. *Dalton Trans.* **2020**, *49*, 4710–4724. [[CrossRef](#)]
11. Yang, Y.Y.; He, M.Q.; Li, M.X.; Huang, Y.Q.; Chi, T.; Wang, Z.-X. Ferrimagnetic copper-carboxyphosphinate compounds for catalytic degradation of methylene blue. *Inorg. Chem. Commun.* **2018**, *94*, 5–9. [[CrossRef](#)]
12. Narulkar, D.D.; Patil, A.R.; Naik, C.C.; Dhuri, S.N. Synthesis, characterization, cis-ligand substitution and catalytic alkane hydroxylation by mononuclear nickel(II) complexes stabilized with tetradentate tripodal ligands. *Inorg. Chim. Acta.* **2015**, *427*, 248–258. [[CrossRef](#)]
13. Naeimi, H.; Moradian, M. Encapsulation of copper(I)-Schiff base complex in NaY nanoporosity: An efficient and reusable catalyst in the synthesis of propargylamines via A3-coupling (aldehyde-amine-alkyne) reactions. *Appl. Catal. A* **2013**, *467*, 400–406. [[CrossRef](#)]
14. Myznikov, L.V.; Fisher, A.I.; Dmitrieva, U.N.; Artamonova, T.V.; Zevatskii, Y.E. Novel mixed complexes of copper(II) and ethylenediamine: Synthesis, crystal structure, and catalytic activity in the cross-coupling reaction of 1-phenyl-5H-tetrazole-5-thiol and iodobenzene. *Russ. J. Gen. Chem.* **2018**, *88*, 495–499. [[CrossRef](#)]
15. Wu, X.Y.; Ren, Z.G.; Lang, J.P. Ni(II) tetrakisphosphine complexes as catalysts/initiators in the ring opening polymerization of ϵ -caprolactone. *Dalton Trans.* **2013**, *43*, 1716–1723. [[CrossRef](#)]
16. Rajković, S.; Ašanin, D.P.; Živković, M.D.; Djuran, M.I. Synthesis of different pyrazine-bridged platinum(II) complexes and ¹H NMR study of their catalytic abilities in the hydrolysis of the N-acetylated L-methionylglycine. *Polyhedron* **2013**, *65*, 42–47. [[CrossRef](#)]
17. Chinnaraja, E.; Arunachalam, R.; Choudhary, M.K.; Kureshy, R.I. Binuclear Cu(II) chiral complexes: Synthesis, characterization and application in enantioselective nitroaldol (Henry) reaction. *Appl. Organomet. Chem.* **2016**, *30*, 95–101. [[CrossRef](#)]
18. Mutti, F.G.; Zoppellaro, G.; Gullotti, M.; Santagostini, L. Biomimetic modelling of copper enzymes: Synthesis, characterization, EPR analysis and enantioselective catalytic oxidations by a new chiral trinuclear copper(II) complex. *Eur. J. Inorg. Chem.* **2009**, *4*, 554–566. [[CrossRef](#)]
19. Zhu, L.; Liu, D.; Wu, L.; Feng, W.; Zhang, X.; Wu, J.; Fan, D.; Lü, X.; Lu, R.; Shi, Q. A trinuclear [Zn₃(L)₂(OAc)₂] complex based on the asymmetrical bis-Schiff-base ligand H₂L for ring-opening copolymerization of CHO and MA. *Inorg. Chem. Commun.* **2013**, *37*, 182–185. [[CrossRef](#)]
20. Sreedaran, S.; Bharathi, K.S.; Rahiman, A.K.; Jagadish, L.; Kaviyarasan, V.; Narayanan, V. Synthesis, electrochemical, magnetic, catalytic and antimicrobial studies of N-functionalized cyclam based trinuclear copper(II) and nickel(II) complexes. *J. Incl. Phenom. Macrocyclic Chem.* **2010**, *66*, 297–306. [[CrossRef](#)]
21. Shi, F.; Chen, Y.; Sun, L.; Zhang, L.; Hu, J. Hydroxylation of phenol catalyzed by different forms of Cu-alginate with hydrogen peroxide as an oxidant. *Catal. Commun.* **2012**, *25*, 102–105. [[CrossRef](#)]
22. Penha, E.S.D.; Cabral, E.L.; Gama, T.S.D.; Oliveira, C.A.D. Use of 35% hydrogen peroxide in tooth bleaching in different clinical time intervals: How long does sensitivity last, and at what times is it more exacerbated. *Biochem. J.* **2018**, *34*, 1095–1104. [[CrossRef](#)]
23. Dong, Y.; Duan, C.; Sheng, Q.; Zheng, J. Preparation of Ag@zeolitic imidazolate framework-67 at room temperature for electrochemical sensing of hydrogen peroxide. *Analyst* **2019**, *144*, 521–529. [[CrossRef](#)] [[PubMed](#)]
24. Asghar, A.; Raman, A.A.A.; Daud, W.M.A.W. Advanced oxidation processes for in-situ production of hydrogen peroxide/hydroxyl radical for textile wastewater treatment: A review. *J. Cleaner Prod.* **2015**, *87*, 826–838. [[CrossRef](#)]
25. Al-Sheddi, E.S.; Farshori, N.N.; Al-Oqail, M.M.; Musarrat, J.; Al-Khedhairi, A.A.; Siddiqui, M.A. Protective effect of lepidium sativum seed extract against hydrogen peroxide-induced cytotoxicity and oxidative stress in human liver cells (HepG2). *Pharm. Biol.* **2016**, *54*, 314–321. [[CrossRef](#)] [[PubMed](#)]
26. Radko, M.; Kowalczyk, A.; Mikrut, P.; Witkowski, S.; Mozgawa, W.; Macyk, W.; Chmielarz, L. Catalytic and photocatalytic oxidation of diphenyl sulphide to diphenyl sulfoxide over titanium dioxide doped with vanadium, zinc, and tin. *RSC Adv.* **2020**, *10*, 4023–4031. [[CrossRef](#)]
27. Chen, X.; Yang, J.; Zhang, A.; Liu, H.; Sun, J.; Liu, J.; Meng, F. Pollution characteristics and chemical behaviors of atmospheric hydrogen peroxide. *Res. Environ. Sci.* **2016**, *29*, 334–342. [[CrossRef](#)]

28. Han, Q.; Ni, P.; Liu, Z.; Dong, X.; Wang, Y.; Li, Z.; Liu, Z. Enhanced hydrogen peroxide sensing by incorporating manganese dioxide nanowire with silver nanoparticles. *Electrochem. Commun.* **2014**, *38*, 110–113. [[CrossRef](#)]
29. Salem, I.A.; El-Sheikh, M.; Zaki, A.B. ChemInform abstract: Kinetics and mechanisms of decomposition reaction of hydrogen peroxide in presence of metal complexes. *Int. J. Chem. Kinet.* **2000**, *32*, 643–666. [[CrossRef](#)]
30. Deng, H.H.; Wu, G.W.; He, D.; Peng, H.P.; Liu, A.L.; Xia, X.H.; Chen, W. Fenton reaction-mediated fluorescence quenching of N-acetyl-L-cysteine-protected gold nanoclusters: Analytical applications of hydrogen peroxide, glucose, and catalase detection. *Analyst* **2015**, *140*, 7650–7656. [[CrossRef](#)]
31. Chen, W.; Zhang, F.; Kong, G.; Cai, S.; Wang, W.; Du, J.; Wu, L. Fast decomposition of hydrogen peroxide by Zeolitic imidazolate framework-67 crystals. *Mater. Lett.* **2019**, *239*, 94–97. [[CrossRef](#)]
32. Sheldrick, G.M. SHELXT-integrated space-group and crystal-structure determination. *Acta Cryst.* **2015**, *A71*, 3–8. [[CrossRef](#)] [[PubMed](#)]
33. Sheldrick, G.M. Crystal structure refinement with SHELXL. *Acta Cryst.* **2015**, *71*, 3–8. [[CrossRef](#)]
34. Yin, J. Study of acetone ketal copper ethylenediamine synthetic and catalytic properties. *J. Weifang Univ.* **2015**, *15*, 32–34. [[CrossRef](#)]
35. Zhu, W.; Lin, C.; Zheng, Y.; Zhu, H. Two dinuclear copper(II) coordination polymers constructed from m-hydroxybenzoic acid and N-donor ligands: Synthesis, crystal structures, and magnetic properties. *Transit. Met. Chem.* **2016**, *41*, 87–96. [[CrossRef](#)]
36. Liu, C.; Liu, Y.; Zhang, L.; Jiang, K.; Zhang, L. Two coordination compounds bearing bis(2-dimethylaminoethyl) ether: Syntheses, crystal structures and catalytic application to the Henry reaction. *Chem. Res. Chin. Univ.* **2018**, *34*, 358–362. [[CrossRef](#)]
37. Zhang, L.W.; Li, X.Y.; Kang, Q.P.; Liu, L.Z. Structures and fluorescent and magnetic behaviors of newly synthesized Ni(II) and Cu(II) coordination compounds. *Crystals* **2018**, *8*, 173. [[CrossRef](#)]
38. Karthik, K.; Qadir, A.M. Synthesis and crystal structure of a new binuclear copper(II) carboxylate complex as a precursor for copper(II) oxide nanoparticles. *J. Struct. Chem.* **2019**, *60*, 1126–1132. [[CrossRef](#)]
39. Yan, X.; Wang, B.; Ma, H.; Gao, F. Synthesis and catalytic properties of transition metal complexes with unsymmetrical Schiff base. *Chem. Res. J. Appl.* **2006**, *18*, 621–624. [[CrossRef](#)]



© 2020 by the authors. Licensee MDPI, Basel, Switzerland. This article is an open access article distributed under the terms and conditions of the Creative Commons Attribution (CC BY) license (<http://creativecommons.org/licenses/by/4.0/>).